

- and scanned at a resolution of ~74 pixels per probe cell. Two scans were collected: a fluorescein scan was obtained with a 515- to 545-nm band-pass filter, and a phycoerythrin scan with a 560-nm long-pass filter. Signals were separated to remove spectral overlap and average counts per cell determined.
14. Each 2.5-kb target sequence was PCR-amplified directly from genomic DNA with the primer pair L14675-T3 (5'-aattaacctactaaagggATCTCGCACGGACTACAAC) and H667-T7 (17).
  15. To scale the sample to the reference intensities, we constructed a histogram of the base 10 logarithm of the intensity ratios for each pair of probes. The histogram had a mesh size of 0.01 and was smoothed by replacing the value at each point with the average number of counts over a five-point window centered at that point. The highest value in the histogram was located, and the resulting intensity ratio was taken to be the most probable calibration coefficient.
  16. Base identification was accomplished with a Bayesian classification algorithm based on variable kernel density estimation. The likelihood of each identification associated with a set of hybridization intensity values was computed by comparing an unknown set of probes to a set of example cases for which the correct base identification was known. The resulting four likelihoods were then normalized so that they summed to 1. Data from both strands were combined by averaging the values. If the most likely base identification had an average normalized likelihood greater than 0.6, it was called, otherwise the base was called as an ambiguity. The example set was derived from two different samples, ib013 and ief005, which have a total of 35 substitutions relative to mt1, of which 19 are shared with the 12 samples analyzed and 16 are not. Identification performance was not sensitive to the choice of examples.
  17. To provide an independently determined reference sequence, each 2.5-kb PCR amplicon was sequenced on both strands by primer-directed fluorescent chain-terminator cycle sequencing with an ABI 373A DNA sequencer and assembled and manually edited with Sequencher 3.0. The analysis presented here assumes that the sequence amplified from genomic DNA is essentially clonal [R. J. Monnat and L. A. Loeb, *Proc. Natl. Acad. Sci. U.S.A.* **82**, 2895 (1985)] and that its determination by gel-based methods is correct. A frequent length polymorphism at positions 303 to 309 was not detected by hybridization under the conditions used. It was excluded from analysis and is not part of the set of 180 polymorphisms discussed in the text. However, polymorphisms at this site have previously been differentiated by oligonucleotide hybridization [M. Stoneking, D. Hedgecock, R. G. Higuchi, L. Vigilant, H. A. Erlich, *Am. J. Hum. Genet.* **48**, 370 (1991)].
  18. The  $P^0$  intensity footprints were detected in the following way: The reference and sample intensities were normalized (15), and  $R$ , the average of  $\log(P^0_{reference}/P^0_{sample})$  over a window of five positions, centered at the base of interest, was calculated for each position in the sequence. Footprints were detected as regions having at least five contiguous positions with a reference or sample intensity at least 50 counts above background and an  $R$  value in the top 10th percentile for the experiment. At 205 polymorphic sites, where the sample was mismatched to  $P^0$ , the mean  $R$  value was 1.01, with a standard deviation of 0.57. At 35,333 nonpolymorphic sites (that is, where both reference and sample had a perfect match to  $P^0$ ) the mean value was -0.05, with a standard deviation of 0.25.
  19. R. L. Cann, M. Stoneking, A. C. Wilson, *Nature* **325**, 31 (1987); M. Zeviani *et al.*, *Am. J. Hum. Genet.* **47**, 904 (1990); D. C. Wallace, *Annu. Rev. Biochem.* **61**, 1175 (1992); S. Horai, K. Hayasaka, R. Kondo, K. Tsugane, N. Takahata, *Proc. Natl. Acad. Sci. U.S.A.* **92**, 532 (1995); T. Hutchin and G. Cortopassi, *ibid.*, p. 6892.
  20. Long-range PCR amplification was carried out on genomic DNA with Perkin-Elmer GeneAmp XL PCR reagents according to the manufacturer's protocol. Primers were L14836-T3 (5'-aattaacctactaaagggATGAAACTTCGGCTCACTCTTGCGC) and RH1066-T7 (5'-taatcagactcatatagggATTCATCATGCGGA-GATGTTGGATGG), based on RH 1066 [S. Cheng, R. Higuchi, M. Stoneking, *Nature Genet.* **7**, 350 (1994)]. Each 100- $\mu$ l reaction contained 0.2  $\mu$ M concentration of each primer and ~10 to 50 ng of total genomic DNA. Transcription reactions were carried out in 10  $\mu$ l with Ambion MAXscript kit according to the manufacturer's protocol. The concentration of the 16.6-kb PCR template was ~2 nM, and the reaction contained Ambion 1 $\times$  biotin-14-CTP/NTP mix and 0.2 mM biotin-16-UTP. Incubation was at 37°C for 2 hours. Fragmentation and hybridization were as described (13), except that 3.5 M TMACI and the biotin-labeled oligonucleotide 5'-CTGAACGGTAGCATCTTGAC were used in the hybridization buffer, which also contained fragmented baker's yeast RNA (100  $\mu$ g/ml) (Sigma). Hybridization was carried out at 40°C for 4 hours.
  21. A custom telecentric objective lens with a numerical aperture of 0.25 focuses 5 mW of 488-nm argon laser light to a 3- $\mu$ m-diameter spot, which is scanned by a galvanometer mirror across a 14-mm field at 30 lines per second. Fluorescence collected by the objective is descanned by the galvanometer mirror, filtered by a dichroic beamsplitter (555 nm) and a band-pass filter (555 to 607 nm), focused onto a confocal pinhole, and detected by a photomultiplier. Photomultiplier output is digitized to 12 bits. A 4096 by 4096 pixel image is obtained in less than 3 min. Pixel size is 3.4  $\mu$ m. The data from four sequential scans were summed to improve the signal-to-noise ratio.
  22. M. D. Brown, A. S. Voljavec, M. T. Lott, I. Mac-Donald, D. C. Wallace, *FASEB J.* **6**, 2791 (1992).
  23. Mitochondrial DNA populations can contain more than one sequence type, in a condition known as heteroplasmy. The LHON mutations shown in Fig. 3C were characterized as being homoplasmic by conventional sequencing and restriction endonuclease digestion (M. Brown, personal communication). In controlled mixing experiments, we have shown that sequences present at the level of 10% can easily be detected by hybridization (M. Chee and R. Yang, unpublished results; N. Shen, personal communication). The sensitivity of detection is sequence dependent. Importantly, hybridization can be used to detect heterozygous nuclear DNA sequences (J. Hacia *et al.*, in preparation).
  24. D. J. Lockhart *et al.*, *Nature Biotech.*, in press.
  25. We thank M. Brown and D. Wallace for the gift of the LHON sample and R. Ward for the 10 African samples, M. Trulson for assistance in two-color hybridization, P. Fiekowsky for image analysis, and P. Berg and E. Lander for comments on the manuscript. R. Davis contributed to the initial concepts in oligonucleotide tiling. We especially thank L. Stryer for his incessant and persistent encouragement. Supported in part by Human Genome grant 5R01HG00813 from NIH (S.P.A.F.).

5 April 1996; accepted 26 July 1996

## An Asymmetric Model for the Nucleosome: A Binding Site for Linker Histones Inside the DNA Gyres

Dmitry Pruss, Blaine Bartholomew, Jim Persinger, Jeffrey Hayes, Gina Arents, Evangelos N. Moudrianakis, Alan P. Wolffe\*

Histone-DNA contacts within a nucleosome influence the function of trans-acting factors and the molecular machines required to activate the transcription process. The internal architecture of a positioned nucleosome has now been probed with the use of photo-activatable cross-linking reagents to determine the placement of histones along the DNA molecule. A model for the nucleosome is proposed in which the winged-helix domain of the linker histone is asymmetrically located inside the gyres of DNA that also wrap around the core histones. This domain extends the path of the protein superhelix to one side of the core particle.

The nucleosome has an active role in gene regulation. Mutations of the core histones have specific consequences for the transcription of particular genes (1). The specificity of these effects can be explained both by the positioning of histones with respect to DNA sequence (2) and the potential

targeting of histone modifications to particular nucleosomes (3). Thus, an understanding of nucleosomal architecture is central to understanding the transcription process.

The nucleosome contains two molecules of each of the four core histones (H2A, H2B, H3, and H4), a single molecule of a linker histone (H1, H1<sup>o</sup>, or H5), and ~180 base pairs (bp) of DNA (4). In isolation, the core histones assemble into an octameric complex (5), whose structure has been determined at 3.1 Å resolution (6–8). The exact path of DNA on the surface of the histone octamer, the position of the linker histone molecule within the nucleosome, and the path of linker DNA between adjacent nucleosomes (9–11) remain to be determined.

We used positioned nucleosomes containing the *Xenopus borealis* somatic 5S ribosomal RNA (rRNA) gene to examine

D. Pruss and A. P. Wolffe, Laboratory of Molecular Embryology, National Institute of Child Health and Human Development, National Institutes of Health, Building 6, Room B1A-13, Bethesda, MD 20892-2710, USA. B. Bartholomew and J. Persinger, Department of Medical Biochemistry, Southern Illinois University at Carbondale, School of Medicine, Carbondale, IL 62901-4413, USA. J. Hayes, Department of Biochemistry, School of Medicine and Dentistry, University of Rochester, Rochester, NY 14642, USA.

G. Arents and E. N. Moudrianakis, Department of Biology, Johns Hopkins University, Baltimore, MD 21218, USA.

\*To whom correspondence should be addressed. E-mail: awlme@helix.nih.gov

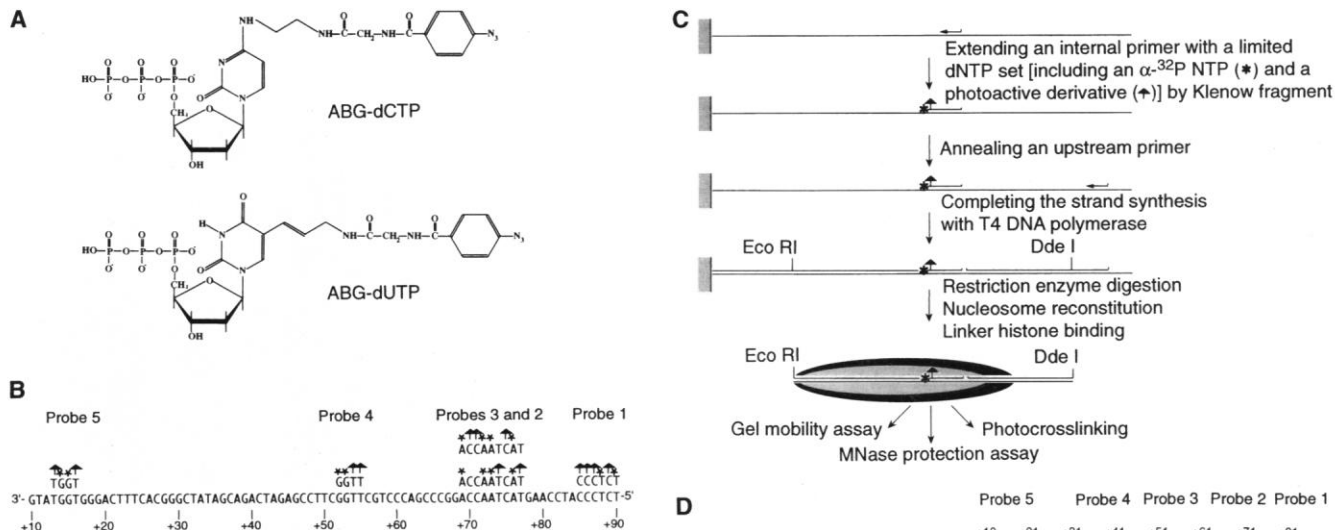


**Fig. 1.** Design of the photoactive probes. **(A)** Photoactive DNA precursors. **(B)** Positions of the photoactive bases (arrows) and <sup>32</sup>P-labeled nucleotides (asterisks) within the bottom strand of 5S rRNA gene. The photoreactive group is attached to the bottom of the major groove by a 1.3-nm linker. **(C)** Synthesis and analysis of the photoactive probes and strategy of nucleosome analysis. The specifically positioned nicks in the labeled strand proved to be very useful for the precise nucleosome position mapping. **(D)** Approximate positions of the photoactive azido moieties with respect to the surface of the histone octamer (shaded) within nucleosomes.

nucleosomal architecture (12, 13). On reconstitution into the nucleosome, linker histones bind preferentially to nucleosomal DNA compared to naked DNA (13). The protection of linker DNA from micrococcal nuclease digestion after incorporation of the linker histone is asymmetric and occurs without any detectable alteration in deoxyribonuclease I cleavage (13). Zero length histone-DNA cross-linking also suggests an asymmetric position for linker histones at the edge of the nucleosome (11). To further test this asymmetric positioning of linker histones in the nucleosome, we introduced broad specificity photoaffinity probes specific for the major groove of DNA (Fig. 1A), at defined points, together with radioactive nucleosides within the *Xenopus* 5S rRNA gene (15) (Fig. 1B). These radiolabeled DNA sequences were subsequently reconstituted into nucleosomes (16) and assayed for structural integrity (17), before the histones were cross-linked to DNA (18) (Fig. 1, C and D).

Gel retardation was used to demonstrate the equivalent reconstitution into nucleosome cores of all five DNA fragments containing distinct radiolabeled photoaffinity probes (Fig. 2A). Linker histones were titrated into the nucleosome, and their preferential interaction with DNA wrapped around a histone octamer was monitored (Fig. 2B). A level of linker histone corresponding to approximately one molecule per two nucleosomes, which allows nucleosome reconstitution with minimal binding of linker histone to naked DNA (Fig. 2B,

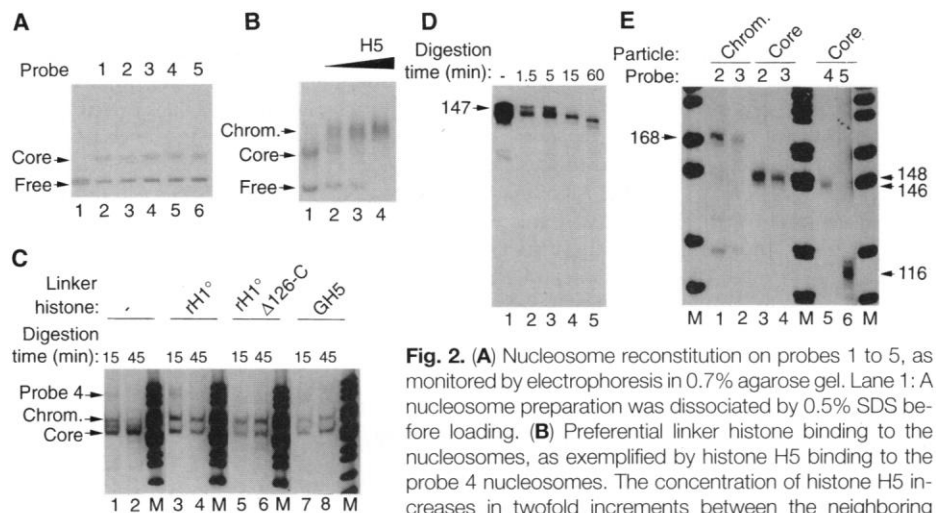


**Fig. 2.** **(A)** Nucleosome reconstitution on probes 1 to 5, as monitored by electrophoresis in 0.7% agarose gel. Lane 1: A nucleosome preparation was dissociated by 0.5% SDS before loading. **(B)** Preferential linker histone binding to the nucleosomes, as exemplified by histone H5 binding to the probe 4 nucleosomes. The concentration of histone H5 increases in twofold increments between the neighboring lanes. Lane 2 represents the experimental sample used in the cross-linking experiments in which there is one molecule of linker histone per two nucleosomes in the reaction. These conditions minimize the potential for linker histone association with naked DNA (13). **(C)** Chromatin barrier assay. Native electrophoresis of probe 4 nucleosome MNase digestion products. Full-length (lanes 3 and 4) and truncated (lanes 5 to 8) linker histones are equally capable of stably protecting ~168-bp-long DNA (Chrom.) from micrococcal nuclease. In the absence of linker histones (lanes 1 and 2) the transiently appearing 165- and 155-bp intermediates are quickly trimmed to the core particle size (Core). **(D)** The unique 5S nucleosome core position remains unchanged during the MNase digestion. Denaturing electrophoresis of probe 4 nucleosome MNase digestion products. The length of the labeled strand changes by merely one to two nucleotides over the course of digestion. **(E)** Denaturing electrophoresis of nucleosome core- (146 to 148 bp) and chromatosome-sized DNA (168 bp) derived from probes 2, 3, 4, and 5. The shorter labeled strands derived from probes 4 and 5 (146 and 116 nucleotides, respectively), resulting from the internal position of the probe-specific nicks within the 5S nucleosome core.

lane 2), was used in subsequent experiments. Several linker histones, chicken erythrocyte H5, and recombinant *Xenopus* histone H1<sup>o</sup> (19) were used. Each linker histone consists of a globular “winged-

helix” central domain flanked by basic NH<sub>2</sub>- and COOH-terminal tail domains (20, 21). Controlled proteolysis or expression of mutant proteins allowed us to examine the contribution of these different do-

mains to nucleosome structure. An additional 20 bp of linker DNA contiguous to the nucleosome core were protected from digestion with micrococcal nuclease by three different mutant proteins: recombinant H1<sup>o</sup>, recombinant H1<sup>o</sup> Δ126-C that lacks most of the COOH-terminal tail domain, and the globular (winged-helix) domain of histone H5 (GH5) (Fig. 2C). As a control, we demonstrated that the photoaffinity probes were positioned at the anticipated sites within the 5S nucleosome. Each nucleosome was trimmed to a core particle containing ~147 bp of DNA by controlled digestion with micrococcal nuclease (for example, Fig. 2D). We then denatured the DNA and mapped the distance of the radiolabeled nucleotide from the edge of the core particle (Fig. 2E). The DNA fragment sizes obtained indicated the predominance of a single nucleosomal position with respect to DNA sequence (Fig. 2E).

After confirming that the five nucleosomes had the anticipated structural properties and were thus reconstituted correctly, we mapped the DNA interactions with the core and linker histones within the 5S nucleosomes. We directly compared histone-DNA contacts made by three different forms of linker histone with three of the probes in the 5S nucleosome (Fig. 3). Whereas cross-linking the entire H1<sup>o</sup> protein to nucleosomal DNA occurred with approximately equivalent efficiency to all of these probes (Fig. 3, asterisks), contacts with recombinant H1<sup>o</sup> Δ126-C, which lack most of the COOH-terminal tail (Fig. 3), were reduced from a high level for probe 2 to a low level for probe 5. This effect was even more pronounced for GH5 (Fig. 3), reflecting the local structural role for this domain in the nucleosome. A more detailed comparison of the cross-linking of histone H5 (Fig. 4A) with that of GH5 (Fig. 4B)

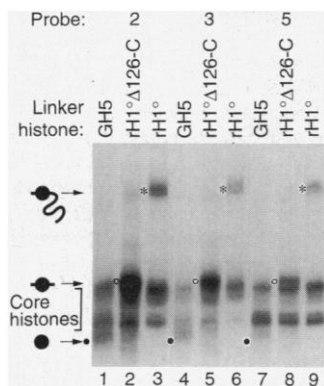


**Fig. 3.** Photocrosslinking-mediated histone labeling in chromatosomes containing globular domain of histone H5 (GH5, closed circles), histone H1<sup>o</sup> with a 72-amino acid deletion in the COOH-terminal tail (H1<sup>o</sup>Δ126-C, open circles), and full-length recombinant histone H1<sup>o</sup> (asterisks).

reveals that GH5 shows selective cross-linking to probes 2 and 3 compared with probes 1, 4, and 5. The relative efficiency of cross-linking of GH5 to DNA in the 5S nucleosome (Table 1, shown schematically in Fig. 4C) revealed a preference for major groove contacts 60 to 68 bp from the dyad axis. This places a favored site for contact with the linker histone well within the nucleosome core, a region of the nucleosome in which DNA is also wrapped on the surface of the core histones.

We explored the structural implications of placing GH5 at this highly asymmetric position within the nucleosome. The structure of GH5 was modeled at this site within the nucleosome core particle. In this modeling, a number of simultaneously applied constraints influenced the positioning of GH5 relative to both DNA and the histone core of the nucleosome. The crystal structure of GH5 has been determined to 2.5 Å resolution (20); however, a structure for the complex between GH5 and DNA has yet to be determined. In our modeling, we chose an orientation of GH5 with respect to the DNA which simulated that of the HNF3-DNA configuration, as a result of the high degree of structural homology between GH5 and HNF3 (21). The location of GH5 along the major groove of the nucleosomal DNA was constrained by our current results and earlier data suggesting a specific cross-link between GH5 and the 5S nucleosomal DNA (12) about 64 bp from the dyad axis.

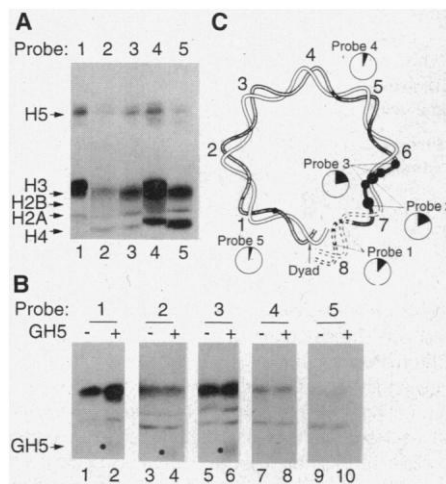


**Fig. 4.** Photocrosslinking-mediated <sup>32</sup>P labeling of histones within nucleosome cores and chromatosomes containing (A) full-length histone H5 and (B) globular domain of histone H5. The globular domain (GH5) is indicated by closed circles. (C) Relative efficiency of photocrosslinking. Closed circles: positions of photoactive nucleotides with the 5S nucleosome. The sizes of the circles correspond to the average GH5 cross-linking yield per photoreactive base of the probe (Table 1). The pie diagrams show the ratio of GH5 (black) and total core histone (white) cross-linking.

If GH5-DNA interactions are analogous to those of HNF3-DNA—that is, GH5 binds within the major groove of DNA—then the

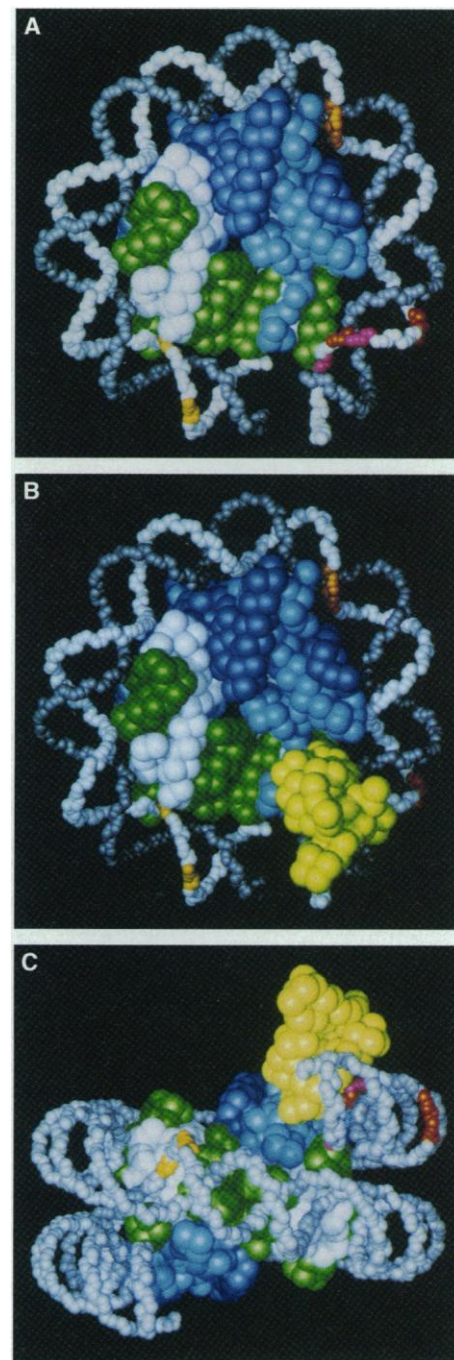


**Fig. 5.** Model for interaction of the globular domain of H5 with the nucleosome core. (A) The locations of the probes used in the cross-linking experiments are marked by a color gradient on one strand (light gray) of the DNA; they progress from the nucleosomal dyad to the edge of the nucleosome, from gold (probe 5) to orange (probe 4), red (probe 3), fuchsia (probe 2), and red (probe 1) again. Core histones are shown: H3 (green), H4 (white), H2B (dark blue), and H2A (light blue). (B) View of the complex down the protein superhelical axis. GH5 (yellow) is at the lower right sector. (C) View of the complex down the molecular two-fold axis with GH5 (yellow) at the upper right sector.

globular domain will not be centered at the nucleosomal dyad (22), because at that place the major groove of the nucleosomal DNA faces the histone octamer, and only the minor groove faces out and is available for additional interactions (with H5) (10).

The GH5 location we propose generates a definite asymmetry in the nucleosome (Fig. 5). The locations of the probes used in the cross-linking experiments are marked (Fig. 5A). One view shown of the complex is down the axis of the protein superhelix of the core. GH5 (yellow) is close to the volume occupied by H2A (light blue) and the exit site of the nucleosomal DNA (Fig. 5B). The particular orientation of GH5 in the major groove chosen allows close contact with histone H2A (23) and extends the path of the protein superhelix of the core. Another portion of GH5 appears to generate an extended protein ramp that might direct a kink in the DNA path (24). The COOH-terminal tail of the GH5 protein points along the double helix at the very edge of the nucleosome core and in the direction of the adjacent nucleosome in the chromatin fiber. The other view shown is of the GH5-nucleosome core complex from above the molecular twofold axis, with GH5 (yellow) at the upper right-hand sector of the picture (Fig. 5C). In this model, part of the GH5 hangs out of the nucleosomal domain and may provide a unique docking element for the interactions with other macromolecular effectors.

Our model for the nucleosome has several implications for chromatin structure and function. An asymmetric nucleosome might

impart a directionality to the folding of the chromatin fiber, consistent with a polar head-to-tail arrangement of linker histone molecules (25). The proposed orientation of the winged-helix domain would favor interaction of the basic COOH-terminal tail of the linker histone with linker DNA, facilitating chromatin compaction (26). A second presumed DNA binding site for the winged-helix domain (20) does not interact with nucleosomal DNA in our model, but it might interact with the DNA of adjacent nucleosomal units of the chromatin fiber, facilitating the assembly of higher order structures. The binding of the winged-helix domain in the major groove could account for sequence selectivity of nucleosome positioning and restriction of nucleosome mobility that are dependent on linker histones (27). Removal of histone H1 as seen on transcriptional activation of inducible promoters (28) would remove a major positional signal for chromatin organization, and the resulting mobility of histone octamers with respect to DNA sequence could greatly facilitate transcriptional activation.

REFERENCES AND NOTES

1. M. Grunstein *et al.*, *J. Cell Sci.* **19**, 29 (1995); W. Kruger *et al.*, *Genes Dev.* **9**, 2770 (1995).
2. A. Almer, H. Rudolph, A. Hinnen, W. Horz, *EMBO J.* **5**, 2689 (1986); H. Richard-Foy and G. L. Hager, *ibid.* **6**, 2321 (1987); R. T. Simpson, *Nature* **343**, 387 (1990); C. Schild, F.-X. Claret, W. Wahli, A. P. Wolffe, *EMBO J.* **12**, 423 (1993); Q. Li and O. Wrangé, *Mol. Cell. Biol.* **15**, 4375 (1995).
3. J. E. Brownell *et al.*, *Cell* **84**, 843 (1996); J. Taunton, C. A. Hassig, S. L. Schreiber, *Science* **272**, 408 (1996).
4. R. Kornberg, *Science* **184**, 868 (1974); \_\_\_\_\_ and J. O. Thomas, *ibid.*, p. 865; M. Noll and R. D. Kornberg, *J. Mol. Biol.* **109**, 393 (1977); F. Caron and J. O. Thomas, *ibid.* **146**, 513 (1981); K. Nightingale, D. Pruss, A. P. Wolffe, *J. Biol. Chem.* **271**, 7090 (1996).
5. T. H. Eickbusch, and E. N. Moudrianakis, *Biochemistry* **17**, 4955 (1978).
6. G. Arents, R. W. Burlingame, B. W. Wang, W. E. Love, E. N. Moudrianakis, *Proc. Natl. Acad. Sci. U.S.A.* **88**, 10148 (1991).
7. G. Arents and E. N. Moudrianakis, *ibid.* **90**, 10489 (1993).
8. \_\_\_\_\_, *ibid.* **92**, 11170 (1995).
9. K. E. van Holde, *Chromatin* (Springer-Verlag, New York, 1988).
10. T. J. Richmond, T. Rechsteiner, K. Luger, *Cold Spring Harbor Symp. Quant. Biol.* **58**, 265 (1993).
11. D. Pruss, J. J. Hayes, A. P. Wolffe, *BioEssays* **17**, 161 (1995).
12. J. J. Hayes, T. D. Tullius, A. P. Wolffe, *Proc. Natl. Acad. Sci. U.S.A.* **87**, 7405 (1990); J. J. Hayes, D. J. Clark, A. P. Wolffe, *ibid.* **88**, 6829 (1991); J. J. Hayes, D. Pruss, A. P. Wolffe, *ibid.* **91**, 7817 (1994).
13. J. J. Hayes and A. P. Wolffe, *ibid.* **90**, 6415 (1993).
14. D. Pruss and A. P. Wolffe, *Biochemistry* **32**, 6810 (1993).
15. Single-stranded biotinylated 5S DNA template (top strand between the positions -113 and +218 relative to the transcription start site) was synthesized with a 5'-biotinylated primer (-113. . . -96, 5'-ATTTCACACAGGAACAG-3') and plasmid pXP10 (12), linearized by Hind III. Probes were synthesized as described (29), with the following modifications: the 5'-biotinylated template strand of 5S DNA was immobilized on streptavidin-agarose before primer extensions, and the ligation of nicks was omitted (Fig. 1).

16. Nucleosome cores were reconstituted onto radiolabeled DNA fragments by salt-dilution exchange with chicken erythrocyte core particles (12). The original 1 M NaCl 60- $\mu$ l exchange reaction contained donor chromatin (5  $\mu$ g), naked nonspecific DNA (1  $\mu$ g), and photoactive labeled 5S fragment (50 fmol). Reconstitution was monitored by electrophoresis in 0.7% agarose gel in 0.5  $\times$  TBE [1 $\times$  tris-borate EDTA (2.5 consists of 90 mM tris base, 90 mM boric acid, 2.5 mM EDTA)]. After electrophoresis, the gels were dried and autoradiographed. Approximately 25 ng of reconstituted nucleosomes, including ~0.25 fmol of a photoprobe-containing nucleosome, were incubated with or without various amounts of linker histones in 10  $\mu$ l of binding buffer [10 mM tris-HCl (pH 8.0), 50 mM NaCl, 0.1 mM EDTA, 5% (v/v) glycerol, 0.05% Triton X-100]. Samples were incubated at room temperature for 15 min and loaded onto 0.7% agarose gels in 0.5 $\times$  TBE, as described above. To avoid potential complications with nonspecific linker histone binding, we subsequently used linker histones (H1<sup>+</sup>, H5)/nucleosome ratios of about 0.5, as confirmed by the titration experiment described above. For the deletion mutant H1 $\Delta$ 126-C and for the globular domain of histone H5, it was not possible to follow their binding to nucleosomes by gel mobility-shift (13), so we used a linker histone amount corresponding to 25% of the amount sufficient to cause extensive DNA aggregation in the samples, based on the observation that the full-length linker histones cause DNA aggregation at ~2:1 ratio to the nucleosomes.
17. Chromatin samples (200 ng) with or without linker histones were diluted fivefold by 10 mM tris-HCl (pH 8.0), 2 mM CaCl<sub>2</sub>, and digested with 2 ng of micrococcal nuclease (MNase) for 5 to 60 min at room temperature. Digestion was terminated by the addition of EDTA (5 mM), SDS (0.25% w/v), and DNA was deproteinized by proteinase K (1  $\mu$ g/ml) (37°C, 30 min), phenol-extracted, and ethanol-precipitated. Digestion products were resolved on 9% acrylamide gel in 1 $\times$  TBE, and core particle and chromatosome-sized bands were excised and electroeluted (90 V, 25 min) and loaded on a sequencing gel.
18. The samples were adjusted to 15 mM NaCl and photocross-linked by mild ultraviolet irradiation. Cross-linked DNA was chemically digested by 70% formic acid, 2% diphenylamine (70°C, 20 min), so that only 5',3'-phosphorylated oligopyrimidine blocks remained covalently bound to the histones. The reactants were extracted by 10 volumes of ether (twice). The samples were freeze-dried, loaded to 15% SDS gel, stained with Coomassie blue to reveal unlabeled protein positions, dried, and autoradiographed.
19. S. Khochbin and A. P. Wolffe, *Eur. J. Biochem.* **225**, 501 (1994).
20. V. Ramakrishnan, J. T. Finch, V. Graziano, P. L. Lee, R. M. Sweet, *Nature* **362**, 219 (1993).
21. K. L. Clark, E. H. Halay, E. Lai, S. K. Burley, *ibid.* **364**, 412 (1993).
22. J. Allan, P. G. Hartman, C. Crane-Robinson, F. X. Aviles, *ibid.* **288**, 675 (1980).
23. T. Boulikas, J. M. Wiseman, W. T. Garrard, *ibid.* **77**, 127 (1980).
24. A. Hamiche, P. Schultz, V. Ramakrishnan, P. Oudet, A. Prunell, *J. Mol. Biol.* **257**, 30 (1996).
25. A. C. Lennard and J. O. Thomas, *EMBO J.* **4**, 3455 (1985).
26. D. J. Clark and T. Kimura, *J. Mol. Biol.* **211**, 883 (1990).
27. G. Meerssemann, S. Pennings, E. M. Bradbury, *ibid.* **220**, 89 (1991); K. Ura, J. J. Hayes, A. P. Wolffe, *EMBO J.* **14**, 3752 (1995); S. Pennings, G. Meerssemann, E. M. Bradbury, *Proc. Natl. Acad. Sci. U.S.A.* **91**, 10275 (1994); J. Yaneva, G. P. Schroth, K. E. van Holde, J. Zlatanova, *ibid.* **92**, 7060 (1995).
28. E. H. Bresnick, M. Bustin, V. Marsaud, H. Richard-Foy, G. L. Hager, *Nucleic Acids Res.* **20**, 273 (1992).
29. B. Bartholomew, G. A. Kassavets, E. P. Geiduschek, *Mol. Cell. Biol.* **11**, 5181 (1991); B. Bartholomew, D. Durkovich, G. A. Kassavets, E. P. Geiduschek, *ibid.* **13**, 942 (1993).
30. We thank the referees for useful comments and T. Vo for preparation of the manuscript.

30 May 1996; accepted 2 August 1996

**Table 1.** The histone harboring covalently attached, <sup>32</sup>P-labeled oligopyrimidine blocks derived from the products of photocrosslinking of GH5-bound nucleosomes were separated by SDS electrophoresis (Fig. 4A); the bands were scanned and the effective yield of photocrosslinking per N-(p-azidobenzoyl)-glycyl(ABG)-modified base was calculated by dividing the band volume by the number of arylazido moieties per residual oligopyrimidine block (arrow) and the number of radioactive phosphates per residual oligopyrimidine block (asterisk). The following labeled blocks can be derived from the probes (Fig. 1B): 1-<sup>ABG</sup>C<sup>ABG</sup>C<sup>ABG</sup>C<sup>T</sup><sup>ABG</sup>C<sup>T</sup> (+85. . .+90), 2-<sup>ABG</sup>dUC and <sup>ABG</sup>dU (+74. . .+75, +77, respectively), 3-<sup>ABG</sup>C<sup>ABG</sup>C and <sup>T</sup><sup>ABG</sup>C (+70. . .+71 and +74. . .+75, respectively), 4-<sup>ABG</sup>dU<sup>ABG</sup>dU (+54. . .+55), 5-<sup>ABG</sup>dU (+16) (the <sup>ABG</sup>dU residue at position +13 does not give rise to any labeled oligopyrimidine block).

Probe	*	↑	Yield per photoactive base			
			GH5	H4	H2A	H2B+H3
1	2	4	1.1	1.3	0.5	6.4
2	1	2	7.1	7.2	4.3	21.2
3	1	3	5.6	2.9	3.9	13.8
4	1	2	2.4	9.0	5.7	24.9
5	1	1	3.6	37.0	7.4	39.2